First Demonstration of Electrostatic Damping of Parametric Instability at Advanced LIGO

Carl Blair *et al.* (LSC Instrument Authors)

Phys. Rev. Lett. **118**, 151102 — Published 11 April 2017

DOI: 10.1103/PhysRevLett.118.151102

First Demonstration of Electrostatic Damping of Parametric Instability at Advanced LIGO

Carl Blair[1],* Slawek Gras[2], Richard Abbott[5], Stuart Aston[3], Joseph Betzwieser[3], David Blair[1], Ryan DeRosa[3], Matthew Evans[2], Valera Frolov[3], Peter Fritschel[2], Hartmut Grote[4], Terra Hardwick[5], Jian Liu[1], Marc Lormand[3], John Miller[2], Adam Mullavey,[3], Brian O'Reilly[3], and Chunnong Zhao[1]

[1] *University of Western Australia, Crawley, Western Australia 6009, Australia*
[2] *Massachusetts Institute of Technology, Cambridge, Massachusetts 02139, USA*
[3] *LIGO Livingston Observatory, Livingston, Louisiana 70754, USA*
[4] *Max Planck Institute for Gravitational Physics, 30167 Hannover, Germany*
[5] *California Institute of Technology, Pasadena 91125, USA*
and
[6] *Louisiana State University, Baton Rouge, Louisiana 70803, USA*

B. P. Abbott,[1] T. D. Abbott,[2] C. Adams,[3] R. X. Adhikari,[1] S. B. Anderson,[1] A. Ananyeva,[1] S. Appert,[1] K. Arai,[1] S. W. Ballmer,[4] D. Barker,[5] B. Barr,[6] L. Barsotti,[7] J. Bartlett,[5] I. Bartos,[8] J. C. Batch,[5] A. S. Bell,[6] G. Billingsley,[1] J. Birch,[3] S. Biscans,[1,7] C. Biwer,[4] R. Bork,[1] A. F. Brooks,[1] G. Ciani,[10] F. Clara,[5] S. T. Countryman,[8] M. J. Cowart,[3] D. C. Coyne,[1] A. Cumming,[6] L. Cunningham,[6] K. Danzmann,[11,12] C. F. Da Silva Costa,[10] E. J. Daw,[13] D. DeBra,[14] R. DeSalvo,[15] K. L. Dooley,[16] S. Doravari,[3] J. C. Driggers,[5] S. E. Dwyer,[5] A. Effler,[3] T. Etzel,[1] T. M. Evans,[3] M. Factourovich,[8] H. Fair,[4] A. Fernández Galiana,[7] R. P. Fisher,[4] P. Fulda,[10] M. Fyffe,[3] J. A. Giaime,[2,3] K. D. Giardina,[3] E. Goetz,[12] R. Goetz,[10] C. Gray,[5] K. E. Gushwa,[1] E. K. Gustafson,[1] R. Gustafson,[17] E. D. Hall,[1] G. Hammond,[6] J. Hanks,[5] J. Hanson,[3] G. M. Harry,[18] M. C. Heintze,[3] A. W. Heptonstall,[1] J. Hough,[6] K. Izumi,[5] R. Jones,[6] S. Kandhasamy,[16] S. Karki,[19] M. Kasprzack,[2] S. Kaufer,[11] K. Kawabe,[5] N. Kijbunchoo,[5] E. J. King,[20] P. J. King,[5] J. S. Kissel,[5] W. Z. Korth,[1] G. Kuehn,[12] M. Landry,[5] B. Lantz,[14] N. A. Lockerbie,[21] A. P. Lundgren,[12] M. MacInnis,[7] D. M. Macleod,[2] S. Márka,[8] Z. Márka,[8] A. S. Markosyan,[14] E. Maros,[1] I. W. Martin,[6] D. V. Martynov,[7] K. Mason,[7] T. J. Massinger,[4] F. Matichard,[1,7] N. Mavalvala,[7] R. McCarthy,[5] D. E. McClelland,[22] S. McCormick,[3] G. McIntyre,[1] J. McIver,[1] G. Mendell,[5] E. L. Merilh,[5] P. M. Meyers,[23] R. Mittleman,[7] G. Moreno,[5] G. Mueller,[10] J. Munch,[20] L. K. Nuttall,[4] J. Oberling,[5] P. Oppermann,[12] Richard J. Oram,[3] D. J. Ottaway,[20] H. Overmier,[3] J. R. Palamos,[19] H. R. Paris,[14] W. Parker,[3] A. Pele,[3] S. Penn,[24] M. Phelps,[6] V. Pierro,[15] I. Pinto,[15] M. Principe,[15] L. G. Prokhorov,[25] O. Puncken,[12] V. Quetschke,[26] E. A. Quintero,[1] F. J. Raab,[5] H. Radkins,[5] P. Raffai,[27] S. Reid,[28] D. H. Reitze,[1,10] N. A. Robertson,[1,6] J. G. Rollins,[1] V. J. Roma,[19] J. H. Romie,[3] S. Rowan,[6] K. Ryan,[5] T. Sadecki,[5] E. J. Sanchez,[1] V. Sandberg,[5] R. L. Savage,[5] R. M. S. Schofield,[19] D. Sellers,[3] D. A. Shaddock,[22] T. J. Shaffer,[5] B. Shapiro,[14] P. Shawhan,[29] D. H. Shoemaker,[7] D. Sigg,[5] B. J. J. Slagmolen,[22] B. Smith,[3] J. R. Smith,[30] B. Sorazu,[6] A. Staley,[8] K. A. Strain,[6] D. B. Tanner,[10] R. Taylor,[1] M. Thomas,[3] P. Thomas,[5] K. A. Thorne,[3] E. Thrane,[31] C. I. Torrie,[1] G. Traylor,[3] G. Vajente,[1] G. Valdes,[26] A. A. van Veggel,[6] A. Vecchio,[32] P. J. Veitch,[20] K. Venkateswara,[33] T. Vo,[4] C. Vorvick,[5] M. Walker,[2] R. L. Ward,[22] J. Warner,[5] B. Weaver,[5] R. Weiss,[7] P. Weßels,[12] B. Willke,[11,12] C. C. Wipf,[1] J. Worden,[5] G. Wu,[3] H. Yamamoto,[1] C. C. Yancey,[29] Hang Yu,[7] Haocun Yu,[7] L. Zhang,[1] M. E. Zucker,[1,7] and J. Zweizig[1]

(LSC Instrument Authors)

(LSC Collaboration)

(Dated: February 13, 2017)

Interferometric gravitational wave detectors operate with high optical power in their arms in order to achieve high shot-noise limited strain sensitivity. A significant limitation to increasing the optical power is the phenomenon of three-mode parametric instabilities, in which the laser field in the arm cavities is scattered into higher order optical modes by acoustic modes of the cavity mirrors. The optical modes can further drive the acoustic modes via radiation pressure, potentially producing an exponential buildup. One proposed technique to stabilize parametric instability is active damping of acoustic modes. We report here the first demonstration of damping a parametrically unstable mode using active feedback forces on the cavity mirror. A 15,538 Hz mode that grew exponentially with a time constant of 182 sec was damped using electro-static actuation, with a resulting decay time constant of 23 sec. An average control force of 0.03 nN rms was required to maintain the acoustic mode at its minimum amplitude.

Introduction Three-mode parametric instability (PI) has been a known issue for advanced laser interferometer gravitational wave detectors since first recognised by Braginsky et al [1], and modelled in increasing detail [2–6]. This optomechanical instability was first observed in 2009 in microcavities [7], then in 2014 in an 80 m cavity [8] and soon afterwards during the commissioning of Advanced LIGO [9]. Left uncontrolled PI results in the optical cavity control systems becoming unstable on time scales of tens of minutes to hours [9].

The first detection of gravitational waves was made by two Advanced LIGO laser interferometer gravitational wave detectors with about 100 kW of circulating power in their arm cavities [10]. To achieve this power level required suppression of PI through thermal tuning of the higher-order mode eigen-frequency [2] explained later in this paper. This tuning allowed the optical power to be increased in Advanced LIGO from about 5 % to 12 % of the design power, sufficient to attain a strain sensitivity of $10^{-23}\,\mathrm{Hz}^{-\frac{1}{2}}$ at 100 Hz.

At the design power (800 kW) it will not be possible to avoid instabilities using thermal tuning alone for two reasons. First the parametric gain scales linearly with optical power and second the acoustic mode density is so high that thermal detuning for one acoustic mode brings other modes into resonance [2, 9].

Several methods are likely to be useful for controlling PI. Active thermal tuning will minimize the effects of thermal transients [11, 12] and maintain operation near the parametric gain minimum. In the future, acoustic mode dampers attached to the test masses [13] could damp acoustic modes. Active damping [14] of acoustic modes can also suppress instabilities, by applying feedback forces to the test masses.

In this letter we report on the control of a PI by actively damping a 15.54 kHz acoustic mode of an Advanced LIGO test mass using electro-static force actuators.

Parametric Instability The parametric gain R_m, as derived by Evans et al [4] is given by:

$$R_\mathrm{m} = \frac{8\pi Q_\mathrm{m} P}{M\omega_\mathrm{m}^2 c\lambda_0} \sum_{n=1}^{\infty} \mathcal{R}e[G_\mathrm{n}] B_\mathrm{m,n}^2. \qquad (1)$$

Here Q_m is the quality factor (Q) of the mechanical mode m, P is the power in the fundamental optical mode of the cavity, M is the mass of the test mass, c is the speed of light, λ_0 is the wavelength of light, ω_m is the mechanical mode angular frequency, G_n is the transfer function for an optical field leaving the test mass surface to the field incident on that same surface and $B_\mathrm{m,n}$ is the spatial overlap between the optical beat note pressure distribution and the mechanical mode surface deformation.

To understand the phenomena, it is instructive to consider the simplified case of a single cavity and a single optical mode. For a simulation analysis including arms and recycling cavities see [4, 5] and for an explanation of dynamic effects that may make high parametric gains from the recycling cavities less likely see [8]. In the simplified case we consider the TEM_{03} mode as it dominates the optical interaction with the acoustic mode investigated here. Equation 2 defines corresponding optical transfer function:

$$\mathcal{R}e[G_{03}] = \frac{c}{L\pi\gamma(1+\Delta\omega^2/\gamma^2)}. \qquad (2)$$

Here γ is the half-width at half maximum of the TEM_{03} optical mode frequency distribution, L is the length of the cavity, $\Delta\omega$ is the spacing in frequency between the mechanical mode ω_m and the beat note of the fundamental and TEM_{03} optical modes. In general the parametric gain changes the time constant of the mechanical mode as in Equation 3:

$$\tau_\mathrm{pi} = \tau_\mathrm{m}/(1-R_\mathrm{m}). \qquad (3)$$

Where τ_m is the natural time constant of the mechanical mode and τ_pi is the time constant of the mode influenced by the opto-mechanical interaction. If the parametric gain exceeds unity the mode becomes unstable. Thermal tuning was used to control PI in Advanced LIGO's Observation run 1 and was integral to this experiment, so will be examined in some detail.

Thermal tuning is achieved using radiative ring heaters that surround the barrel of each test mass without physical contact as in Figure 1. Applying power to the ring heater decreases the radius of curvature of the mirrors. This changes the cavity g-factor and tunes the mode spacing between the fundamental (TEM_{00}) and higher order transverse electromagnetic (TEM_{mn}) modes in the

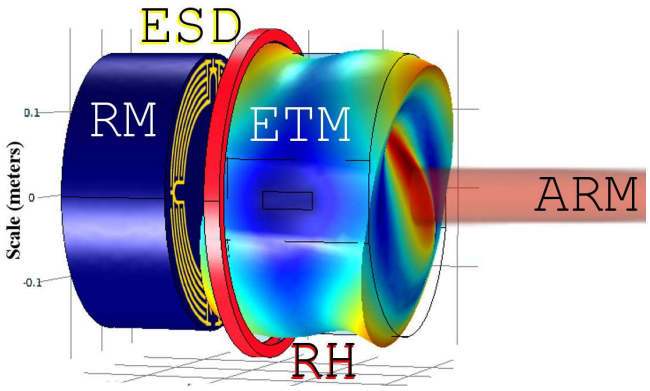

FIG. 1. Schematic of the gold ESD comb on the reaction mass (RM), the ring heater (RH) and the end test mass (ETM) with exaggerated deformation due to the 15,538 Hz mode. The colour represents the magnitude of the displacement (red is large, blue is small). The laser power in the arm cavity is depicted in red (ARM). Suspension structures are not shown and while the scale is marked to the left the distance between RM and ETM is exaggerated by a factor of 10

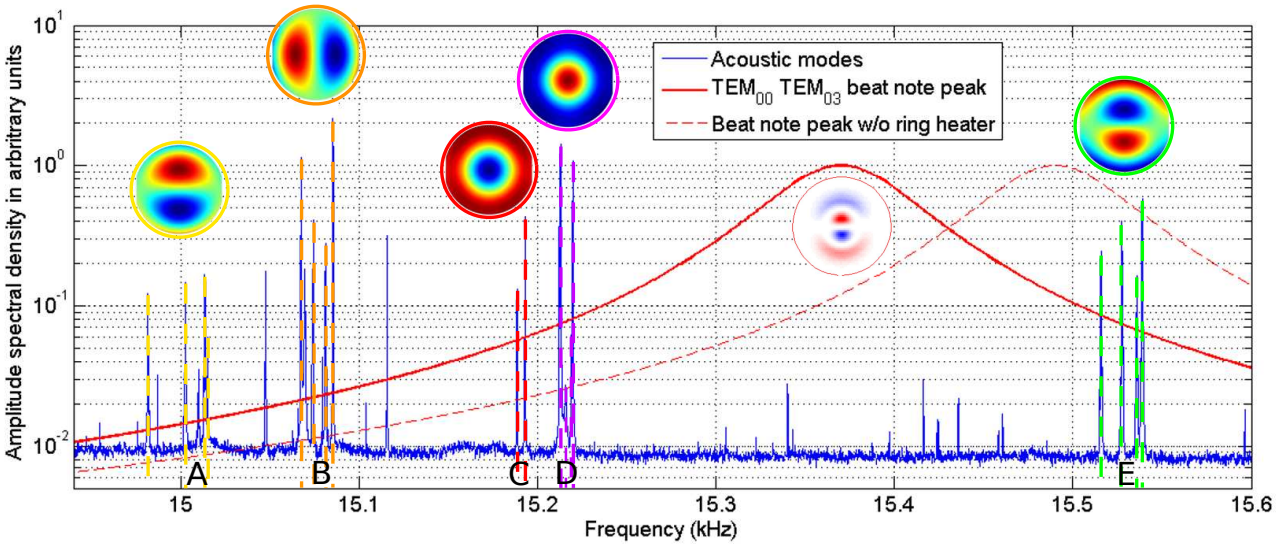

FIG. 2. The relative location of the optical and mechanical modes during Advanced LIGO Observation run 1. Mechanical modes measured in transmission of the Output mode cleaner shown in blue with mode surface deformation generated from FEM modeling overlay-ed. These modes appear in groups of four, one for each test mass. They have line-width ~ 1 mHz. The optical transfer function for a simplified single cavity is shown in bold red with the ring heater on and turned off in dashed red. The shape of the TEM_{03} mode simulated with OSCAR [15] is inset below the peak.

cavity, thereby tuning the parametric gain by changing $\Delta\omega$ in Equation 2.

Figure 2 shows five groups of mechanical modes and the optical transfer function (Equation 2) for the TEM_{03} mode. The ring heater tuning used during Advanced LIGOs first observing run [16] is shown in bold red. Without thermal tuning, the peak in the optical transfer function moves to higher frequency (dashed red), decreasing the frequency spacing $\Delta\omega$ with mechanical mode group E. This leads to the instability of this group of modes. (Note that the mirror acoustic mode frequencies are only weakly tuned by heater power, due to the small value of the fused silica temperature dependence of Young's modulus).

If the ring heater power is increased inducing approximately 5 m change in radius of curvature, the optical transfer function peak in Figure 2 moves left about 400 Hz, decreasing the value $\Delta\omega$ for mode group A, resulting in their instability. The mode groups C and D are stable as the second and fourth order optical modes that might be excited from these modes are far from resonance. Mode Group B is also stable at the circulating optical power used in this experiment presumably due to either lower quality factor $Q_{\rm m}$ or lower optical gain G_{30} of the TEM_{30} mode as investigated in [17]. Extrapolating from Equation 2 and the observed parametric gain, increasing the interferometer power by a factor of 3 results in no stable region. Mode group A at 15.00 kHz and group E at 15.54 kHz will be unstable simultaneously.

Electrostatic Control Electrostatic control of PI was proposed [18] and studied in the context of the LIGO electrostatic control combs by Miller et al [14]. Here we report studies of electrostatic feedback damping for the group E modes at 15.54 kHz.

The main purpose of the electrostatic drive (ESD) is to provide longitudinal actuation on the test masses for lock acquisition [19] and holding the arm cavities on resonance. It creates a force between the test masses and their counterpart reaction masses, through the interaction of the fused silica test masses with the electric fields generated by a comb of gold conductors that are deposited on the reaction mass. The physical locations of these components are depicted in Figure 1. Detail of the gold comb is shown in Figure 3 along with the force density on the test mass.

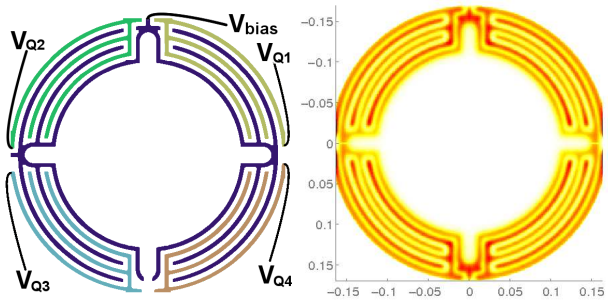

FIG. 3. The ESD comb pattern printed on the reaction mass (left) and the force distribution on the test mass (right) with the same voltage on all quadrants

The force applied to the test mass $F_{\rm ESD}$ is dominated by the dipole attraction of the test mass dielectric to the

electric field between the electrodes of the gold comb. $F_{\rm app,m}$ is the fraction $b_{\rm m}$ of this force that couples to the acoustic mode:

$$F_{\rm app,m} = b_{\rm m} F_{\rm ESD,Q} = b_{\rm m}\alpha_{\rm Q} \times \frac{1}{2}(V_{\rm bias} - V_{\rm Q})^2. \quad (4)$$

Here $\alpha_{\rm Q}$ is the force coefficient for a single quadrant resulting in a force $F_{\rm ESD,Q}$, while $V_{\rm bias}$ and $V_{\rm Q(1-4)}$ are the voltages of the ESD electrodes defined in Figure 3. The overlap $b_{\rm m}$ between the ESD force distribution $\vec{f}_{\rm ESD,Q}$ and the displacement $\vec{u}_{\rm m}$ of the surface for a particular acoustic mode m can be approximated as a surface integral derived by Miller [14]:

$$b_{\rm m} \approx \Big| \iint_{\mathcal{S}} \vec{f}_{\rm ESD,Q} \cdot (\vec{u}_{\rm m} \cdot \hat{z})\, {\rm d}\mathcal{S}. \Big| \quad (5)$$

If a feedback system is created that senses the mode amplitude and provides a viscous damping force using the ESD, the resulting time constant of the mode $\tau_{\rm esd}$ is given by:

$$\tau_{\rm esd} = \Big(\frac{1}{\tau_{\rm m}} + \frac{K_{\rm m}}{2\mu_{\rm m}}\Big)^{-1}. \quad (6)$$

Here $K_{\rm m}$ is the gain applied between the velocity measurement and the ESD actuation force on a mode with time constant $\tau_{\rm m}$ and effective mass $\mu_{\rm m}$. Reducing the effective time constant lowers the effective parametric gain:

$$R_{\rm eff} = R_{\rm m} \times \frac{\tau_{\rm esd}}{\tau_{\rm m}}. \quad (7)$$

The force required $F_{\rm req}$ to reduce a parametric gain R_m to an effective parametric gain R_{eff} when the mode amplitude is the thermally excited amplitude was used by Miller [14] to predict the forces required from the ESD for damping PI:

$$F_{\rm req} = \frac{x_{\rm m}\mu_{\rm m}\omega_{\rm m}^2}{b_{\rm m}}\Big(\frac{R_{\rm m} - R_{\rm eff}}{Q_{\rm m} R_{\rm eff}}\Big), \quad (8)$$

at the thermally excited amplitude $x_{\rm m} = \sqrt{k_{\rm B}T/\mu_{\rm m}\omega_{\rm m}^2}$, where $k_{\rm B}$ is the Boltzmann constant and T temperature.

Feedback Loop Figure 4 shows the damping feedback loop implemented on the end test mass of the Y-arm (ETMY). The error signal used for mode damping is constructed from a quadrant photodiode (QPD) that receives light transmitted by ETMY. By suitably combining QPD elements, we measure the beat signal between the cavity TEM_{00} mode and the TEM_{03} mode that is being excited by the 15,538 Hz ETMY acoustic mode. This signal is band-pass filtered at 15,538 Hz, then phase shifted to produce a control signal that is 90 degrees out of phase with the mode amplitude (velocity damping). The damping force is applied, with adjustable gain, to two quadrants of the ETMY electro-static actuator. Table I summarises control and cavity parameters

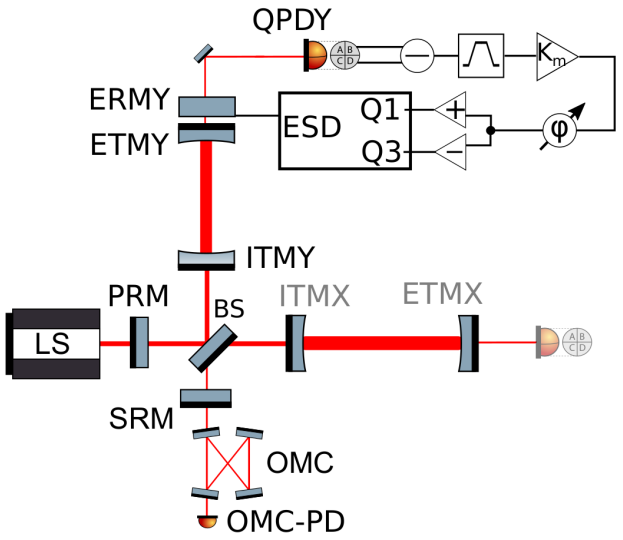

FIG. 4. A simplified schematic of advanced LIGO showing key components for damping PI in ETMY. Components shown include input and end test masses (ITM/ETM), beam-splitter (BS), power and signal recycling mirrors (PRM/SRM), the laser source (LS), quadrant photo-detectors, the output mode cleaner (OMC), the OMC transmission photo-detector (OMC-PD). While 4 reaction masses exist, only the Y end reaction mass is shown (ERMY) with key components of the damping loop. These components generate a signal from the vertical orientation of QPDY, filter the signal with a 10 Hz wide band pass centered on 15,538 Hz , apply gain $K_{\rm m}$ and phase ϕ (digitally controlled) then differentially drive of the upper right $Q1$ and lower left $Q3$ ESD quadrants.

TABLE I. Cavity and control parameters

Symbol	Value	Description
Q_m	12×10^6	Q factor of 15,538 Hz mode
P	100 kW	Power contained in arm cavity
$\omega_m/2\pi$	15,538 Hz	Frequency of unstable mode
M	40kg	mass of test mass
b_m	0.17	effective mass scaled ESD overlap factor for 15,538 Hz mode
λ_0	1064 nm	laser wavelength
α_Q	4.8×10^{-11} N/V^2	ESD quadrant force coefficient
L	4km	Arm cavity length
$V_{\rm bias}$	400V	Bias voltage on ESD
$V_{\rm Q}$	[-20,20]V	ESD control voltage range

Results PI stabilization via active damping was demonstrated by first inducing the ETMY 15,538 Hz to become parametrically unstable. This was achieved by turning off the ring heater tuning, so that the TEM_{03} mode optical gain curve better overlapped this acoustic mode, as shown in Figure 2. When the mode became significantly elevated in the QPD signal, the damping loop was closed with a control gain to achieve a clear damping of the mode amplitude and a control phase optimised to ±15 degrees of viscous damping. The mode amplitude was

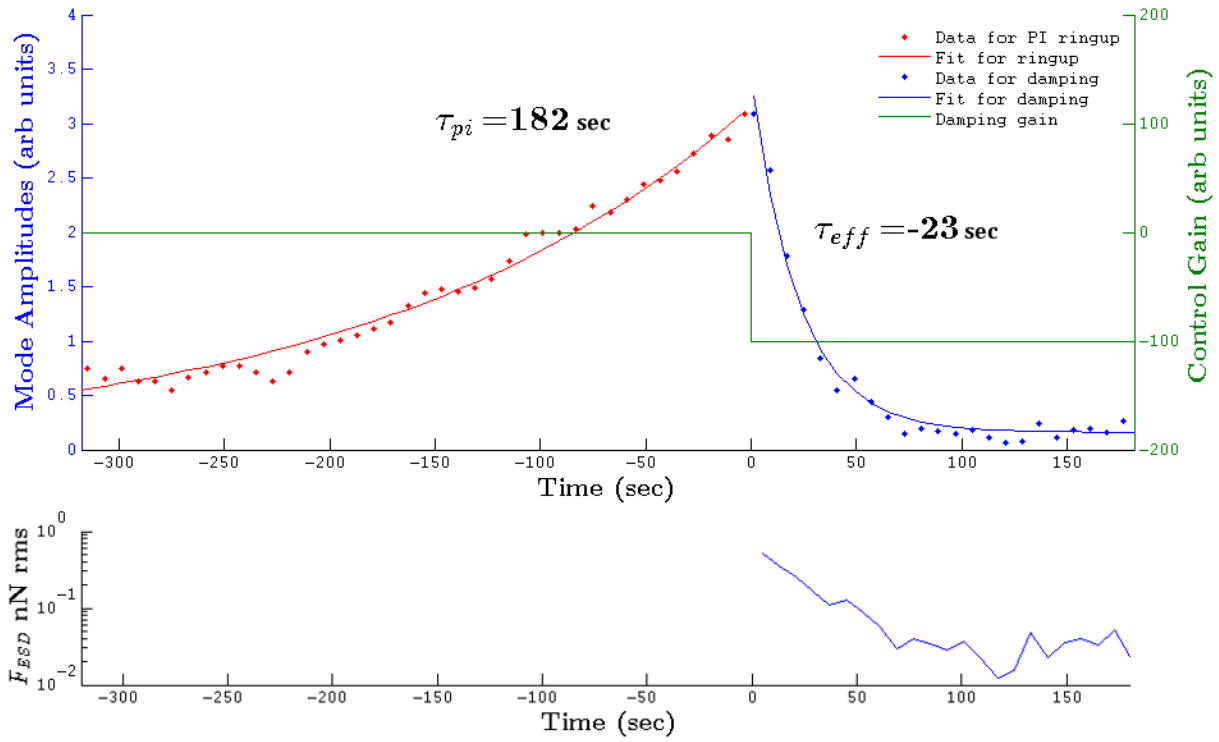

FIG. 5. Damping of parametric instability. Upper panel, the 15,538 Hz ETMY mode is unstable ringing up with a time constant of 182 ± 9 sec and estimated parametric gain of $R_{\rm m} = 2.4$. Then at 0 sec control gain is applied resulting in an exponential decay with a time constant of 23 ± 1 sec and effective parametric gain $R_{\rm eff,m} = 0.18$. Lower panel, the control force over the same period.

monitored using the photodetector at the main output of the interferometer (labelled OMC-PD in Figure 4), as it was found to provide a higher signal-to-noise ratio than the QPD.

The results are shown in Figure 5, which plots the mode amplitude during the unstable ring-up phase with time constant $\tau_{\rm pi}$ 182 sec, followed by the ring-down time constant $\tau_{\rm eff}$ due to optical gain and damping of -23 sec. From the ring-up we estimate the parametric gain to be 2.4 ± 0.8 from Equation 3. With the damping applied:

$$R_{\rm eff} = \frac{R_{\rm m}\tau_{\rm eff}}{\tau_{\rm m} + R_{\rm m}\tau_{\rm eff}} \qquad (9)$$

the effective parametric gain is reduced to a stable value of $R_{\rm eff} = 0.18 \pm 0.06$. The uncertainty is primarily due to the uncertainty in the estimate of τ_m which was obtained by the method described in [9].

At the onset of active damping (time t = 0 in Figure 5), the feedback control signal produces an estimated force of $F_{ESD} = 0.62$ nN rms (at 15,538 Hz). As the mode amplitude decreased the control force dropped to a steady state value of 0.03 nN rms. Over a 20 minute period in this damped state, the peak control force was 0.11 nN peak.

Discussion The force required to damp the 15,538 Hz mode when Advanced LIGO reaches design power can be determined from the ESD force used to achieve the observed parametric gain suppression presented here, combined with the expected parametric gain when operated at high power:

$$\frac{F_{\rm req}}{F_{\rm ESD}} = \frac{R_{\rm eff}}{R_{\rm req}} \frac{R_{\rm max} - R_{\rm req}}{R_m - R_{\rm eff}} \qquad (10)$$

The maximum parametric gain $R_{\rm max}$ where $\Delta\omega = 0$ is calculated using Equation 2. For the 15,538 Hz mode the de-tuning is $\Delta\omega \approx 50\,Hz$ with zero ring heater power, so $R_{\rm max} \approx 7$ for the power level of these experiments. At full design power the maximum gain will be $R_{\rm max} \approx 56$. To obtain a quantitative result, we set a requirement for damping such that the effective parametric gain of unstable acoustic modes after damping be $R_{\rm req} = 0.1$.

Using Equation 10, the measurements of R_m and $R_{\rm eff}$, the maximum force required to maintain the damped state at high power is $F_{\rm ESD} = 1.5$ nN rms. Prior to this investigation Miller predicted [14] that a control force of approximately 10 nN rms would be required to maintain this mode at the thermally excited level.

The PI control system must cope with elevated mode amplitudes as the PI mode may build up before PI control can be engaged. There is therefore a requirement for some safety factor (available voltage / drive voltage

in damped state) such that the control system will not saturate. A safety factor of at least 10 would be prudent. The average ESD drive voltage $V_{Q1} = -V_{Q3}$ over the duration the mode was in the damped state was 0.42 mV rms, however during this time it peaked at ± 1.4 mV peak out of a ±20 V control range, leading to a safety factor of more than 10,000. At high power the safety factor will be reduced by the required force ratio of Equation 10 resulting in an expected safety factor of 310.

As the laser power is increased, other modes are likely to become unstable. The parametric gain of these modes should be less than the gain of mode group E provided the optical transfer function used in these experiments is maintained. However these modes may also have lower spatial overlap b_m with the ESD. Miller's simulation [14] show some modes in the 30-90 kHz range will require up to 30 times the control force F_{ESD} required to damp the group E modes. Even in this situation the PI safety factor is approximately 10.

Coupling of PI control forces presented here to noise in the main interferometer output were insignificant. A detailed investigation will be required when commissioning the complete parametric instability control system.

Conclusion We have shown for the first time electrostatic control of parametric instability. An unstable acoustic mode at 15,538 Hz with a parametric gain of 2.4 ± 0.8 was successfully damped to a gain of 0.18 ± 0.06, using electrostatic control forces. The damping force required to keep the mode in the damped state was 0.03 nN rms. The prediction through FEM simulation was that the ESD would need to apply approximately six times this control force to maintain the mode amplitude at the thermally excited level. At high power it is estimated that damping the 15.54 kHz mode group to an effective parametric gain of 0.1 will result in a safety factor ≈ 310. It is predicted that unstable modes that are most problematic to damp will still have a safety factor of 10.

Acknowledgments The authors acknowledges the entire LIGO Scientific Collaboration for their wide ranging expertise and contributions. LIGO was constructed by the California Institute of Technology and Massachusetts Institute of Technology with funding from the National Science Foundation, and operates under Cooperative Agreement No. PHY-0757058. Advanced LIGO was built under Grant No. PHY-0823459. This paper has LIGO Document Number LIGO-P1600090. The corresponding author was supported by the Australian Research Council and the LSC fellows program.

* carl.blair@uwa.edu.au

[1] V. Braginsky, S. Strigin, and S. Vyatchanin, Physics Letters A **287**, 331 (2001).
[2] C. Zhao, L. Ju, J. Degallaix, S. Gras, and D. G. Blair, Phys. Rev. Lett. **94**, 121102 (2005).
[3] S. Strigin and S. Vyatchanin, Physics Letters A **365**, 10 (2007).
[4] M. Evans, L. Barsotti, and P. Fritschel, Physics Letters A **374**, 665 (2010).
[5] S. Gras, C. Zhao, D. G. Blair, and L. Ju, Classical and Quantum Gravity **27**, 205019 (2010).
[6] S. P. Vyatchanin and S. E. Strigin, Physics-Uspekhi **55**, 1115 (2012).
[7] M. Tomes and T. Carmon, Phys. Rev. Lett. **102**, 113601 (2009).
[8] C. Zhao, L. Ju, Q. Fang, C. Blair, J. Qin, D. Blair, J. Degallaix, and H. Yamamoto, Phys. Rev. D **91**, 092001 (2015).
[9] M. Evans, S. Gras, P. Fritschel, J. Miller, L. Barsotti, D. Martynov, A. Brooks, D. Coyne, R. Abbott, R. X. Adhikari, K. Arai, R. Bork, B. Kells, J. Rollins, N. Smith-Lefebvre, *et al.*, Phys. Rev. Lett. **114**, 161102 (2015).
[10] B. P. Abbott and et al (LIGO Scientific Collaboration and Virgo Collaboration), Phys. Rev. Lett. **116**, 061102 (2016).
[11] Y. Fan, C. Zhao, J. Degallaix, L. Ju, D. G. Blair, B. J. J. Slagmolen, D. J. Hosken, A. F. Brooks, P. J. Veitch, and J. Munch, Review of Scientific Instruments **79** (2008), 10.1063/1.2982239.
[12] J. Ramette, M. Kasprzack, A. Brooks, C. Blair, H. Wang, and M. Heintze, Applied Optics **55**, 2619 (2016).
[13] S. Gras, P. Fritschel, L. Barsotti, and M. Evans, Phys. Rev. D **92**, 082001 (2015).
[14] J. Miller, M. Evans, L. Barsotti, P. Fritschel, M. MacInnis, R. Mittleman, B. Shapiro, J. Soto, and C. Torrie, Physics Letters A **375**, 788 (2011).
[15] J. Degallaix, Journal of Physics: Conference Series **228**, 012021 (2010).
[16] B. P. Abbott, R. Abbott, T. D. Abbott, M. R. Abernathy, F. Acernese, K. Ackley, C. Adams, T. Adams, P. Addesso, R. X. Adhikari, V. B. Adya, C. Affeldt, M. Agathos, K. Agatsuma, N. Aggarwal, *et al.* (LIGO Scientific Collaboration and Virgo Collaboration), Phys. Rev. Lett. **116**, 131103 (2016).
[17] P. Barriga, B. Bhawal, L. Ju, and D. G. Blair, J. Opt. Soc. Am. A **24**, 1731 (2007).
[18] L. Ju, D. G. Blair, C. Zhao, S. Gras, Z. Zhang, P. Barriga, H. Miao, Y. Fan, and L. Merrill, Classical and Quantum Gravity **26**, 015002 (2009).
[19] O. Miyakawa, R. Ward, R. Adhikari, B. Abbott, R. Bork, D. Busby, M. Evans, H. Grote, J. Heefner, A. Ivanov, S. Kawamura, F. Kawazoe, S. Sakata, M. Smith, R. Taylor, M. Varvella, S. Vass, and A. Weinstein, Journal of Physics: Conference Series **32**, 265 (2006).